Carbon Nanospheres

DOI: 10.1002/ange.201303927

Simple and Green Synthesis of Nitrogen-Doped Photoluminescent Carbonaceous Nanospheres for Bioimaging**

Wei Li, Zehui Zhang, Biao Kong, Shanshan Feng, Jinxiu Wang, Lingzhi Wang, Jianping Yang, Fan Zhang, Peiyi Wu, and Dongyuan Zhao**

Carbon nanomaterials, including carbon nanotubes,[1] fullerenes,[2] graphene,[3] and porous carbons,[4] have attracted tremendous attention owing to their unique properties and potential applications, including adsorption, separation, catalysis, gas storage, and electrode materials, among others. More recently, carbon nanomaterials with photoluminescent properties have presented exciting opportunities in the search for benign "nanolanterns" that are highly desired in bioimaging, disease detection, and drug delivery.[5] Compared to organic dyes and fluorescent semiconductor nanocrystals (quantum dots),[6] photoluminescent carbon nanomaterials are superior in chemical inertness and possess distinct benefits, such as no optical blinking, low photobleaching, low cytotoxicity, and excellent biocompatibility.[7] Thus far, numerous approaches, including arc discharge,[8] laser irradiation,[9] electrochemical synthesis,[10] pyrolysis,[11] and hydrothermal[12] methods have been developed to prepare these versatile materials. However, there is still a bottleneck for progress in understanding and controlling the morphology, size, and surface chemistry of the resultant products with high quantum yields (QYs), which impede their practical applications. Moreover, exploration of photoluminescent carbon nanomaterials with high QYs (>30%), for use as fluorescent chemosensors to monitor and image biological processes, still remains in an early stage.[13] It has been demonstrated that functionalizing fluorescent carbon nanomaterials with nitrogen groups can significantly enhance their properties and expand their novel applications.[14] Despite several successes in this area, it is still of great urgency to develop simple and effective methods to synthesize novel nitrogen-doped photoluminescent carbon nanomaterials with uniform morphology and high QYs.

Recently, there has been a trend to synthesize carbon-based materials from biomass materials, as these are inexpensive, easy to obtain, and nontoxic, among other properties.[15] A typical biomass material, more than 480000 tons per year of cocoon silk produced by the *Bombyx mori* silkworm is cultivated all over the world.[16] It is composed of fibrous proteins (fibroin) and sericin, which surrounds the fibroin fibers and cements them together.[17] Moreover, silk fibroin can be easily dissolved and then regenerated into new materials.[18] Herein, we present a simple hydrothermal treatment of cocoon silk to prepare water-soluble, nitrogen-doped, photoluminescent-polymer-like carbonaceous nanospheres (CNSs) in water, without any additives, such as salts, acids, or bases. Our results show that the resultant CNSs possess a uniform morphology, with a size of ca. 70 nm, plentiful oxygen and nitrogen functional groups, and excellent and stable fluorescent properties with a QY of ca. 38%. Moreover, the CNSs can be applied as a fluorescent probe for the detection of Hg^{2+} and Fe^{3+} ions. Mostly important, we further demonstrate that such photoluminescent CNSs exhibit low toxicits and are biocompatible for use with in vivo imaging and as biosensors in living cells, as well as in tissues at a depth of 60–120 μm.

Hydrothermal treatment of cocoon silk at 200 °C leads to a yellow dispersion of the CNSs. A transmission electron microscopy (TEM) image (Figure 1a) shows that the CNSs are uniform in size (an average of ca. 70 nm) and well-dispersed. A dynamic light scattering (DLS) plot (Supporting Information, Figure S1) further demonstrates the monodis-

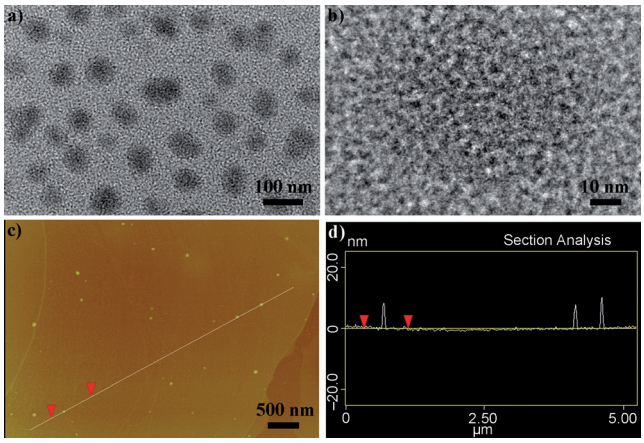

Figure 1. a) TEM image and b) High-resolution TEM image of the polymer-like CNSs. c) AFM topography image of the CNSs on a mica substrate; d) the corresponding height-profile analysis along the line in (c).

[*] W. Li,[+] B. Kong, S. S. Feng, Dr. J. X. Wang, Dr. L. Z. Wang, J. P. Yang, Dr. F. Zhang, Prof. Dr. D. Y. Zhao
Department of Chemistry, and Laboratory of Advanced Materials, Fudan University, Shanghai 200433, (P. R. China)
E-mail: dyzhao@fudan.edu.cn
Homepage: http://www.mesogroup.fudan.edu.cn/
Z. H. Zhang,[+] Prof. Dr. P. Y. Wu
State Key Laboratory of Molecular Engineering of Polymers, Department of Macromolecular Science, Fudan University
Shanghai 200433 (P. R. China)
E-mail: peiyiwu@fudan.edu.cn
[+] These authors contributed equally to this work.

[**] This work was supported by the State Key Basic Research Program of the PRC (2012CB224805, 2013CB934104), and the NSF of China (21210004).
Supporting information for this article is available on the WWW under http://dx.doi.org/10.1002/anie.201303927.

persity of the CNSs, which possess a uniform dynamic size of ca. 90 nm. The high resolution TEM image in Figure 1b clearly reveals that the diffraction contrast of the CNSs is very low and without any obvious lattice fringes, which is indicative of their polymer-like amorphous nature. The structures of the CNSs were further characterized by atom force microscopy (AFM, Figure 1c and d). The images suggest that the CNSs are monodispersed, with a size of ca. 70 nm in diameter, but only ca. 11 nm in height. This height distortion may be attributed to the structure collapse of the CNSs during the preparation process for AFM testing samples, which is in good agreement with the TEM characterizations. It is a common phenomenon that low-polymerization polymers are obtained in a collapsed form when they are dried on solid substrates, but maintain their initial form in solvents.[19]

Chemical and structural information about the CNSs was further obtained from the FTIR spectrum (Figure S2). Peaks at around 3413 cm^{-1} and 3089 cm^{-1} correspond to the OH/NH and C=C–H stretching modes, respectively. Bands at 1595, 1513, and 1456 cm^{-1} can be attributed to the C=C stretching mode of the polycyclic aromatic hydrocarbons, whereas others at 1152 and 1111 cm^{-1} correspond to the asymmetric stretching vibrations of C–NH–C. These results reveal that the molecular structures of the CNSs mainly contain polycyclic aromatic and aromatic CN groups.[14b,20] The presence of plentiful carbonyl units, which, combined with the rich hydroxyl groups on the surface, endows the CNSs with high water solubility and a Zeta potential of −36.8 mV, is illustrated by the characteristic absorption peak at 1636 cm^{-1}. X-ray photoelectron spectroscopy (XPS) was used to investigate the surface states of the CNSs. The survey spectrum (Figure 2a) of the CNSs shows three typical peaks of C_{1s}, N_{1s}, and O_{1s}, and the corresponding content of each element is displayed in the inset in Figure 2a. The spectrum of C_{1s} in the CNSs (Figure 2b) can be deconvoluted into several single peaks that correspond to C–C (284.5 eV), C–N (286.0 eV), C–O (286.5 eV), and C=N/C=O (288.0 eV) functional groups,[21] which are consistent with the FTIR results. The N_{1s} spectrum (Figure 2c) reveals three relative nitrogen species of C–N–C (399.5 eV), N–C_3 (400.6 eV), and N–H (401.5 eV),[21] which have been observed in the case of C_{1s} and FTIR spectra. Moreover, the spectrum of O_{1s} (Figure 2d) further confirms these observations with two characteristic oxygen states of C=O (531.6 eV) and C–O (533.0 eV).[14b] The elemental analysis results (Table S1) further reveal that the CNSs are composed of C (56.34%), H (5.63%), N (12.82%), and O (calculated, 25.21%) atoms, which is consistent with the XPS results. Compared with cocoon silk, the increase in carbon content and decrease in oxygen content indicates sufficient carbonization during the high-temperature treatment. Therefore, we can conclude that the as-prepared CNSs are mainly composed of polycyclic aromatic and aromatic CN species derived from the dehydration and polymerization of amino acids, as well as possessing abundant hydroxyl, amino, and carbonyl/carboxylate groups on their surface.

To gain insight into the formation process of the CNSs, time-dependent experiments were carried out. After hydrothermal treatment at 200°C for 6 h, the uniformly long silk fibers were cut into a number of short microrods (Figures S3a and S3c). The presence of the fibroin fibers suggested that the sericin could be first dissolved in water during the high-temperature treatment (Figures S3b and S3d). After continuous hydrothermal treatment for 24 h, the silk was completely converted into irregular polymeric fragments (Figures S3e and S3f), which indicates that the significant effect of water molecules on the degradation of fibroin fibers, as a result of the subcritical conditions, derives from the hydrothermal treatment at 200°C. However, as the reaction time was extended to 48 h, well-dispersed and uniform polymer aggregates were found with average sizes of ca. 45 nm (Figures S3g and S3h) and without obvious irregular large nanostructures. The ultra-low diffraction contrast of the aggregates illustrates their low-polymerization properties. After another 24 h of hydrothermal treatment, the aggregates became larger and denser, resulting in the CNSs (Figure 1a,b). Based on these observations, we propose an integrated top-down and bottom-up strategy towards the formation of the CNSs (Scheme 1). It is known that cocoon silk consists of two core fibroin fibers coated by sericin,

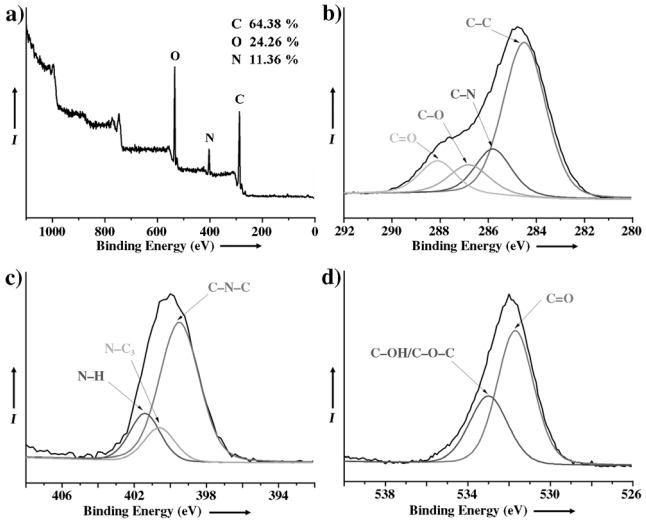

Figure 2. XPS spectra of the polymer-like CNSs. a) Survey spectrum. b) C_{1s} spectrum. c) N_{1s} spectrum. d) O_{1s} spectrum.

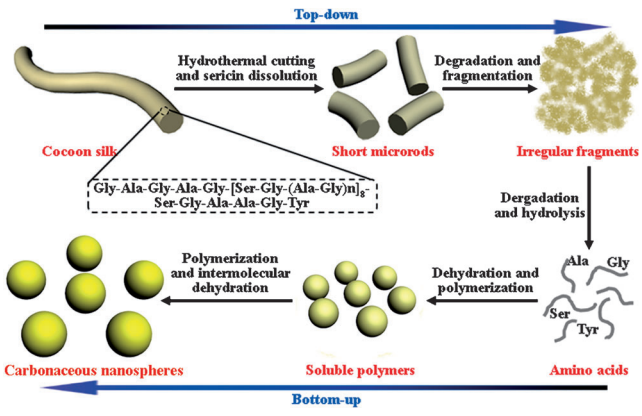

Scheme 1. Integrated top-down and bottom-up strategy for the formation mechanism of polymer-like CNSs.

a water-soluble protein.[17] The fibroin mainly contains glycine (Gly), alanine (Ala), serine (Ser), and tyrosine (Tyr) amino acids (up to 90%), which are found primarily in the repetitive sequence: Gly-Ala-Gly-Ala-Gly-[Ser-Gly-(Ala-Gly)n]$_8$-Ser-Gly-Ala-Ala-Gly-Tyr with weak chemical bonds.[17] In this case, during the initial hydrothermal stage, the sericin first undergoes a dissolution process, as it is strongly solvated by water; simultaneously, the amorphous random regions of the silk fibroin with weak interactions can be easily broken down by the oxidation of water, thus leading to the formation of short microrods.[18] With time, the amorphous- and crystal-dominant structures are gradually degraded into irregular polymeric fragments, and the proteins begin to hydrolyze into small amino acids from the strong solvation effect and high reactivity of water molecules towards weak chemical bonds (such as ester or amido bonds) under such subcritical conditions.[22] When the proteins are fully digested into individual amino acids (Gly, Ala, Ser, Tyr), their concentrations will increase sharply in the system, which then act in situ as molecular precursors for carbon nanomaterials; this is similar to the well-known hydrothermal carbonization process of carbohydrates.[15] As a result, uniform organic aggregates are obtained through the primary dehydration and polymerization of amino acids. As intermolecular dehydration and hydrothermal carbonization proceed, uniform CNSs are finally formed. Therefore, during hydrothermal treatment, the silk first experiences a top-down hydrolysis/degradation process into amino acids, which then undergoes a bottom-up dehydration and polymerization to produce the CNSs.

Figure 3a shows the optical properties of the CNSs. The absorption spectrum shows a clear adsorption feature at ca. 274 nm, which is a typical characteristic of fluorescent carbon dots (CDs).[14c] When excited at 330 nm, the CNSs showed

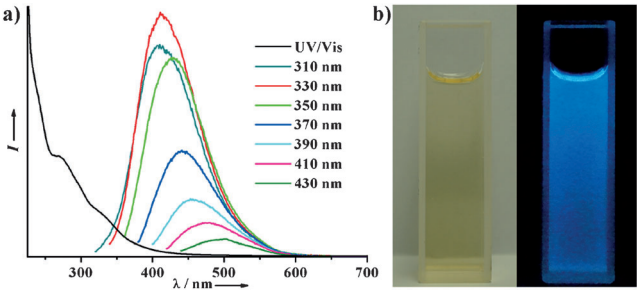

Figure 3. a) UV/Vis absorption spectrum and photoluminescence emission spectra of a dilute aqueous solution of the polymer-like CNSs at different excitation wavelengths. b) Photograph of the dilute aqueous solution of the CNSs kept in air for 1 year at room temperature, and excited by daylight and a UV lamp (365 nm).

strong blue photoluminescence (PL) centered at approximately 414 nm. In addition, the excitation-dependent PL behavior of the CNSs, which is very similar to primarily reported CDs,[7c,11b,12b] can be clearly distinguished. When the excitation wavelength changes from 310 to 430 nm, the PL peak correspondingly shifts from 412 (violet) to 502 nm (green). The bright and colorful PL may be attributed to the synergistic effect of the carbogenic core and the surface/molecular state of the CNSs.[12a,14b,c] The short microrods derived from the hydrothermal process also exhibited excellent photoluminescent properties when excited by UV (340–380 nm), blue (450–490 nm), and green (515–560 nm) light (Figure S4). This indicates that the fluorophores may be present in situ, or form immediately after the hydrothermal treatment, but the exact mechanisms responsible for the PL remain to be elucidated. Ongoing work will be done in detail. The quantum yield was calculated to be ca. 38% at 310 nm excitation, which is much higher than previously reported CDs. This may be caused by the in situ doping by various amine groups (perhaps owing to amide-containing fluorophores).[14a] Even after being kept for 1 year in air at room temperature, the CNSs still exhibited a transparent appearance and strong blue color under UV light (365 nm; Figure 3b), which offers another advantage for their future applications. Moreover, the fluorescence of the CNSs was significantly quenched by Hg^{2+} and Fe^{3+} ions (Figures S5a and S5c), because of the effective coordination/chelation interactions between Hg^{2+}/Fe^{3+} ions and the plentiful hydroxyl, amino, and carbonxylate groups of the CNSs; this may lead to the formation of nonradiative electron-transfer or energy-transfer, thus resulting in the substantial fluorescence quenching.[13b,14a,b] The Hg^{2+} ion dependence plot (Figure S5b) of F/F_0 (F_0 and F are the highest fluorescence intensities of CNSs excited at 330 nm in the absence and presence of metal ions, respectively) showed good linearity with concentrations of Hg^{2+} in the range of 50–250 μM, but the Fe^{3+} ion dependence plot (Figure S5d) exhibited a regular nonlinear trend with concentration. To evaluate the selectivity of this quenching system, we investigated the fluorescence intensity changes of CNSs in the presence of various metal ions under the same conditions, including Al^{3+}, Ca^{2+}, Cr^{3+}, Cu^{2+}, Mg^{2+}, Pb^{2+}, K^+, Ag^+, Ni^{2+}, Co^{2+}, Zn^{2+}, Na^+ and Fe^{2+} (Figure S5e). No tremendous decrease was observed upon addition of these ions into the CNS dispersion, thus indicating a their negligible influence on our fluorescent CNSs as a probe towards Hg^{2+} and Fe^{3+} ions.

For further biological applications, 3-(4,5-dimethylthiazol-2-yl)-2,5-diphenyltetrazolium bromide (MTT) assays were carried out to evaluate the cytotoxicity of the CNSs. The cell viabilities of Hela and 293T cells were tested after being exposed to CNSs at different concentrations (Figure S6). As observed, the cell viabilities of both cells declined by $< 10\%$ upon addition of the CNSs at up to 80 μg mL^{-1}, which suggests that the nanospheres have low cytotoxicity. Furthermore, to determine cell permeability, Hela cells were incubated in Dulbecco's modified Eagle's medium (DMEM) containing 0.04 mg mL^{-1} of the CNSs for 30 min at 37 °C, and washed with phosphate buffer solution (PBS) to remove the remaining extracellular nanospheres. A remarkable intracellular fluorescence is observed in the confocal laser scanning microscopy image (Figure 4a) after the CNSs are incubated with Hela cells. The bright-field and overlapped fluorescence images (Figure 4b,c) reveal that the fluorescence signals are from the perinuclear regions of the cytosol, thus indicating good cell-permeability of the CNSs into living cells. The fluorescent nanospheres were further investigated

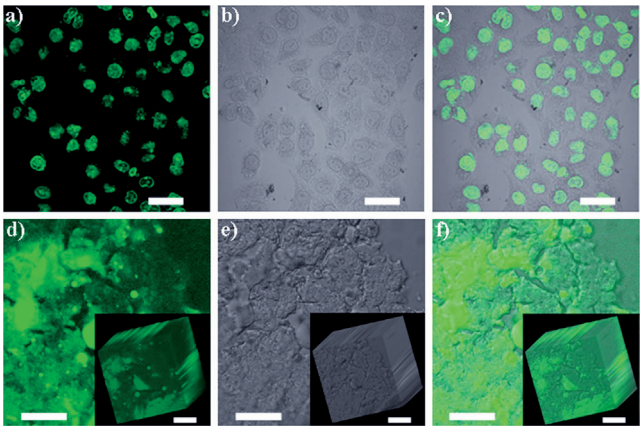

Figure 4. Confocal laser scanning microscopy images, collected from the emission wavelength channel: 475–525 nm (λ_{ex} = 400 nm), of a) Living Hela cells incubated for 30 min at 37 °C in DMEM containing 0.04 mg mL^{-1} of the polymer-like CNSs, and d) human breast cancer (MCF-7) cells tumor tissues treated with 0.04 mg mL^{-1} of the CNSs for 6 hours at 37 °C. b, e) The corresponding bright-field images and c, f) overlapped images of the living cells and the tissues. The inset images in (d–f) are the corresponding 3D confocal fluorescence, bright-field and overlapped images of the tissues accumulated along the *z* direction at a depth of 60–120 μm. All scale bars are 40 μm.

in tissue imaging. The confocal laser fluorescence and corresponding bright-field images (Figure 4 d–f) show that the luminescence intensities are evenly distributed in human breast cancer (MCF-7) tumor tissues, which suggests that the CNSs have good tissue permeability and fluorescent imaging. Moreover, the 3D confocal fluorescence and bright-field images (Figure 4 d–f, insets) accumulated along the *z* direction display relatively homogenous and strong fluorescence intensities over the tissues at a depth of 60–120 μm, which is consistent with above observations. In addition, confocal laser scanning microcopy analysis also indicates the high stability of these CNSs, with no blinking and low bleaching. Thus, these fluorescent nanospheres can be considered to have low toxicity and to be biocompatible for in vivo imaging and biosensors.

In summary, we have reported a simple and green route to synthesize water-soluble and nitrogen-doped polymer-like CNSs with a uniform size of ca. 70 nm on a large scale through hydrothermal treatment of cocoon silk in water. Optical property characterization and cytotoxicity studies indicate that these CNSs display excellent photoluminescent properties, with a high QY of ca. 38 % and low cytotoxicity, which have been successfully used in imaging living cells and MCF-7 cell tissues at a depth of 60–120 μm. Moreover, the CNSs can be applied as a fluorescent probe for the detection of Hg^{2+} and Fe^{3+} ions. Most importantly, we have demonstrated that this method features an integrated top-down and bottom-up growth mechanism for the CNSs, which we believe can be extended to high-throughput design and can be used to synthesize functional carbon nanomaterials from abundant natural biomass materials for versatile applications including in vivo imaging, biosensing, information encryption, and electrical chemistry.

Experimental Section

Preparation of cocoon silk: The cocoon silk was prepared as described elsewhere.[23] Briefly, cocoons of *Bombyx mori* were boiled for 45 min in an aqueous solution of Na_2CO_3 (5 wt %) to remove silk sericin and wax, and then cooled to room temperature. The silks were obtained after being washed with water and ethanol, and then dried at room temperature.

Preparation of carbonaceous nanospheres: The prepared cocoon silk (1.0 g) was mixed with H_2O (20 mL), then added into a 25 mL Teflon-lined autoclave and heated at 200 °C for 72 h. The carbonaceous nanospheres were collected by removing the insoluable materials though simple filtration.

Received: May 8, 2013
Published online: June 20, 2013

Keywords: bioimaging · hydrothermal carbonization · nanostructures · nitrogen doping · photoluminescence

[1] L. Dai, *Angew. Chem.* **2011**, *123*, 4840; *Angew. Chem. Int. Ed.* **2011**, *50*, 4744.
[2] M. Prato, *J. Mater. Chem.* **1997**, *7*, 1097.
[3] J. Liang, Y. Jiao, M. Jaroniec, S. Z. Qiao, *Angew. Chem.* **2012**, *124*, 11664; *Angew. Chem. Int. Ed.* **2012**, *51*, 11496.
[4] a) W. Li, F. Zhang, Y. Q. Dou, Z. X. Wu, H. J. Liu, X. F. Qian, D. Gu, Y. Y. Xia, B. Tu, D. Y. Zhao, *Adv. Energy Mater.* **2011**, *1*, 382; b) W. Li, D. Y. Zhao, *Chem. Commun.* **2013**, *49*, 943.
[5] a) L. Cao, M. J. Meziani, S. Sahu, Y. P. Sun, *Acc. Chem. Res.* **2013**, *46*, 171; b) S. N. Baker, G. A. Baker, *Angew. Chem.* **2010**, *122*, 6876; *Angew. Chem. Int. Ed.* **2010**, *49*, 6726; c) H. Li, Z. Kang, Y. Liu, S.-T. Lee, *J. Mater. Chem.* **2012**, *22*, 24230.
[6] a) P. W. Barone, S. Baik, D. A. Heller, M. S. Strano, *Nat. Mater.* **2005**, *4*, 86; b) X. Michalet, F. F. Pinaud, L. A. Bentolila, J. M. Tsay, S. Doose, J. J. Li, G. Sundaresan, A. M. Wu, S. S. Gambhir, S. Weiss, *Science* **2005**, *307*, 538; c) U. Resch-Genger, M. Grabolle, S. Cavaliere-Jaricot, R. Nitschke, T. Nann, *Nat. Methods* **2008**, *5*, 763.
[7] a) L. Cao, X. Wang, M. J. Meziani, F. S. Lu, H. F. Wang, P. J. G. Luo, Y. Lin, B. A. Harruff, L. M. Veca, D. Murray, S. Y. Xie, Y. P. Sun, *J. Am. Chem. Soc.* **2007**, *129*, 11318; b) D. Y. Pan, J. C. Zhang, Z. Li, M. H. Wu, *Adv. Mater.* **2010**, *22*, 734; c) R. L. Liu, D. Q. Wu, X. L. Feng, K. Mullen, *J. Am. Chem. Soc.* **2011**, *133*, 15221.
[8] X. Y. Xu, R. Ray, Y. L. Gu, H. J. Ploehn, L. Gearheart, K. Raker, W. A. Scrivens, *J. Am. Chem. Soc.* **2004**, *126*, 12736.
[9] S.-L. Hu, K.-Y. Niu, J. Sun, J. Yang, N.-Q. Zhao, X.-W. Du, *J. Mater. Chem.* **2009**, *19*, 484.
[10] a) H. T. Li, X. D. He, Z. H. Kang, H. Huang, Y. Liu, J. L. Liu, S. Y. Lian, C. H. A. Tsang, X. B. Yang, S. T. Lee, *Angew. Chem.* **2010**, *122*, 4532; *Angew. Chem. Int. Ed.* **2010**, *49*, 4430; b) J. G. Zhou, C. Booker, R. Y. Li, X. T. Zhou, T. K. Sham, X. L. Sun, Z. F. Ding, *J. Am. Chem. Soc.* **2007**, *129*, 744.
[11] a) H. P. Liu, T. Ye, C. D. Mao, *Angew. Chem.* **2007**, *119*, 6593; *Angew. Chem. Int. Ed.* **2007**, *46*, 6473; b) R. L. Liu, D. Q. Wu, S. H. Liu, K. Koynov, W. Knoll, Q. Li, *Angew. Chem.* **2009**, *121*, 4668; *Angew. Chem. Int. Ed.* **2009**, *48*, 4598.
[12] a) J. Wang, C.-F. Wang, S. Chen, *Angew. Chem.* **2012**, *124*, 9431; *Angew. Chem. Int. Ed.* **2012**, *51*, 9297; b) S. Qu, X. Wang, Q. Lu, X. Liu, L. Wang, *Angew. Chem.* **2012**, *124*, 12381; *Angew. Chem. Int. Ed.* **2012**, *51*, 12215.
[13] a) B. Kong, A. W. Zhu, C. Q. Ding, X. M. Zhao, B. Li, Y. Tian, *Adv. Mater.* **2012**, *24*, 5844; b) A. W. Zhu, Q. Qu, X. L. Shao, B. Kong, Y. Tian, *Angew. Chem.* **2012**, *124*, 7297; *Angew. Chem. Int. Ed.* **2012**, *51*, 7185.

[14] a) S. Zhu, Q. Meng, L. Wang, J. Zhang, Y. Song, H. Jin, K. Zhang, H. Sun, H. Wang, B. Yang, *Angew. Chem.* **2013**, *125*, 4045; *Angew. Chem. Int. Ed.* **2013**, *52*, 3953; b) S. Liu, J. Tian, L. Wang, Y. Zhang, X. Qin, Y. Luo, A. M. Asiri, A. O. Al-Youbi, X. Sun, *Adv. Mater.* **2012**, *24*, 2037; c) C. Z. Zhu, J. F. Zhai, S. J. Dong, *Chem. Commun.* **2012**, *48*, 9367; d) Y. Li, Y. Zhao, H. H. Cheng, Y. Hu, G. Q. Shi, L. M. Dai, L. T. Qu, *J. Am. Chem. Soc.* **2012**, *134*, 15.

[15] a) M.-M. Titirici, M. Antonietti, *Chem. Soc. Rev.* **2010**, *39*, 103; b) B. Hu, K. Wang, L. Wu, S.-H. Yu, M. Antonietti, M.-M. Titirici, *Adv. Mater.* **2010**, *22*, 813.

[16] Y. S. Yun, S. Y. Cho, J. Shim, B. H. Kim, S.-J. Chang, S. J. Baek, Y. S. Huh, Y. Tak, Y. W. Park, S. Park, H.-J. Jin, *Adv. Mater.* **2013**, *25*, 1993.

[17] a) H. J. Jin, J. Park, V. Karageorgiou, U. J. Kim, R. Valluzzi, P. Cebe, D. L. Kaplan, *Adv. Funct. Mater.* **2005**, *15*, 1241; b) R. Nazarov, H. J. Jin, D. L. Kaplan, *Biomacromolecules* **2004**, *5*, 718.

[18] D. M. Phillips, L. F. Drummy, D. G. Conrady, D. M. Fox, R. R. Naik, M. O. Stone, P. C. Trulove, H. C. De Long, R. A. Mantz, *J. Am. Chem. Soc.* **2004**, *126*, 14350.

[19] a) P. Valle-Vigón, M. Sevilla, A. B. Fuertes, *Chem. Mater.* **2010**, *22*, 2526; b) Y. Hu, J. Ge, Y. Sun, T. Zhang, Y. Yin, *Nano Lett.* **2007**, *7*, 1832.

[20] M. J. Bojdys, J.-O. Müller, M. Antonietti, A. Thomas, *Chem. Eur. J.* **2008**, *14*, 8177.

[21] Y. Zheng, Y. Jiao, L. Ge, M. Jaroniec, S. Z. Qiao, *Angew. Chem.* **2013**, *125*, 3192; *Angew. Chem. Int. Ed.* **2013**, *52*, 3110.

[22] A. T. Quitain, H. Daimon, K. Fujie, S. Katoh, T. Moriyoshi, *Ind. Eng. Chem. Res.* **2006**, *45*, 4471.

[23] Y. H. Yang, Z. Z. Shao, X. Chen, P. Zhou, *Biomacromolecules* **2004**, *5*, 773.

